Materials Advances

ROYAL SOCIETY OF CHEMISTRY

PAPER

View Article Online
View Journal | View Issue

Check for updates

Cite this: *Mater. Adv.*, 2025, 6, 8574

Modifying the electronic structure of hematite to be an efficient adsorbent for the removal of 2,4-dichlorophenoxyacetic acid from water and food samples

Befkad Tedla Belayneh,[ab] Bekele Getahun,[b] Taame Abraha Berhe,[c]
Belete Asefa Aragaw,[d] Zerihun Getaneh Workneh[e] and
Amare Aregahegn Dubale *[a]

The widespread use of 2,4-dichlorophenoxyacetic acid (2,4-D) in agriculture has raised significant health and environmental concerns, highlighting the need for effective removal techniques. In this study, we propose a strategy to modify the electronic structure by doping zinc into the hematite structure (ZDH) *via* a hydrothermal method for the removal of 2,4-D from real samples. The synthesized adsorbent was thoroughly characterized using XRD, FTIR, SEM, elemental mapping, and XPS to confirm structural and surface modifications. The highest adsorption capacity for 2,4-D was found to be 123.5 mg g^{-1} when using the 4% Zn-doped hematite (ZDH4) adsorbent. The adsorption of 2,4-D was best explained by the Langmuir isotherm model, while the kinetics were best described by the pseudo-second-order model. The ΔH° of +65.6 kJ mol^{-1} indicated an endothermic process and a chemisorption mechanism, while the negative ΔG° values confirmed that the adsorption process is spontaneous. The as-prepared adsorbent exhibited remarkable reusability, maintaining up to 95% efficiency after four cycles of adsorption–desorption processes. ZDH4 achieved impressive adsorptive removal efficiencies of 98.9%, 99.2%, and 99.6% when applied to real samples, including river water, onion, and potato, respectively, using 60 mg of adsorbent at pH 3. The adsorption mechanism was primarily attributed to hydrogen bonding, electrostatic interactions, and van der Waals forces, as evidenced by post-characterization using FTIR, XPS, and XRD. This study highlights the design of a highly efficient adsorbent for removing pollutants from aqueous environments and real samples.

Received 30th August 2025,
Accepted 13th October 2025

DOI: 10.1039/d5ma00985e

rsc.li/materials-advances

1. Introduction

All living things depend on water for survival, making its quality making a global concern. The primary causes of water quality issues are industrial effluents, which contain harmful substances such as pesticides, dyes, transition metals, and other organic contaminants.[1–3] Even small quantities of these pollutants can pose significant risks to aquatic ecosystems, wildlife, and human health, as water pollution can quickly enter the food supply chain.[4,5] Pesticides and herbicides pose significant threats to both environmental and human health.[6–8] Among these agrochemicals, 2,4-D is a prominent weed killer linked to various diseases.[9–11] Furthermore, 2,4-D persists in aquatic habitats, contaminating water bodies.[12,13] It is primarily used to keep fruits and vegetables fresh while eliminating weeds.[6] Due to its chemical properties, 2,4-D accumulates in soil, seeps into groundwater, and enters the food chain, impacting both humans and animals.[14–16] The WHO Guidelines classify 2,4-D as a moderately hazardous herbicide due to its hepatogenic and carcinogenic properties, as well as its potential to induce cell death.[17,18] The guidelines specify that drinking water should not contain more than 30 μg L^{-1} of 2,4-D, underscoring the necessity of removing it from water sources.[7,19]

Removing 2,4-D from water bodies is an urgent ecological issue due to its toxicity to aquatic life and its tendency to accumulate in the food chain.[20–23] Various techniques have

---

[a] *Center for Material Science and Engineering, College of Natural and Computational Science, Addis Ababa University, Addis Ababa 1176, Ethiopia. E-mail: amare.aregahegn@aau.edu.et*
[b] *Department of Chemistry, College of Natural and Computational Sciences, Dilla University, P. O. Box 419, Dilla, Ethiopia*
[c] *Department of Chemistry, College of Natural and Computational Sciences, Adigrat University, P. O. Box 50, Adigrat, Ethiopia*
[d] *Department of Chemistry, College of Sciences, Bahir Dar University, P. O. Box 79, Bahir Dar, Ethiopia*
[e] *School of Civil and Environmental Engineering, College of Technology and Built Environment, Addis Ababa University, Addis Ababa 1176, Ethiopia*

been employed for this purpose, including photocatalytic degradation, electrochemical degradation, ozone oxidation, biodegradation, adsorption, membrane filtration, and the Fenton method.[24–27] Among these, adsorption is the most widely used strategy for removing 2,4-D from water and food samples. It is cost-effective, energy-efficient, user-friendly, offers high removal efficiency, saves time, and produces minimal harmful byproducts.[28–33]

Many adsorbents, such as activated carbon (AC), graphene and its derivatives, biosorbents, biochar adsorbents, polymer nanocomposites, and metal–organic frameworks, effectively remove 2,4-D through phase adsorption techniques.[34–36] However, recovering used adsorbents for the remediation of aquatic environments poses challenges.[37] Recent studies have underscored the critical role of magnetic adsorption agents in 2,4-D removal, highlighting their growing importance in addressing this issue.[38] In particular, Fe_2O_3 nanomaterials have garnered significant attention due to their hydrophilicity, non-toxicity, chemical stability, and biocompatibility. Iron oxide (Fe_2O_3) nanoparticles are especially valued for their efficient adsorption capabilities and environmental friendliness.[39,40] However, these bare nanoparticles often agglomerate, which diminishes their sorption capacity and surface area.[41] To address this clustering problem, modifying the Fe_2O_3 nanoparticles is essential.

Doping Fe_2O_3 with transition metals such as Zn, Cr, and Ti at the iron sites has proven to be an effective strategy for enhancing photocatalytic and adsorptive capabilities.[42,43] Among these metals, zinc is particularly advantageous due to its similar valence properties to iron. Incorporating Zn^{2+} into the Fe_2O_3 structure improves the stability of the nanoparticles under various biological and environmental conditions.[44] By modulating the electronic structure and surface properties of Fe_2O_3, zinc doping increases the material's surface area for pollutant interaction while simultaneously enhancing its stability and reactivity.[45] To the best of our knowledge, there are no reports of zinc-doped iron oxide nanocomposites being used to remove 2,4-D from water and food.

In this study, we developed a highly efficient Zn-doped Fe_2O_3 material for the adsorptive removal of 2,4-D from water and food samples using a slightly improved simultaneous co-precipitation strategy. We examined the effects of zinc doping on the electronic structure, crystallinity, and morphology of hematite to enhance the removal of 2,4-D from aqueous solutions. Compared to undoped hematite, the hematite doped with 4% Zn exhibits a remarkable adsorption capacity for eliminating 2,4-D from both synthetic solutions and real samples. We investigated the optimization of various parameters, including pH, amount of adsorbent, initial concentration of 2,4-D, agitation speed, contact duration, and the presence of coexisting ions, on adsorption performance. Additionally, we employed various isotherm models, conducted kinetic studies, and performed thermodynamic analyses to explore how 2,4-D interacts with Zn-doped Fe_2O_3. The application of the prepared adsorbent in real samples showed great promise. Finally, we conducted multiple regeneration and reuse experiments to evaluate the stability of Zn-doped Fe_2O_3. This work provides a new direction for designing highly efficient adsorbents for the effective removal of herbicides from water and food samples.

2. Experimental section

2.1. Chemicals and apparatus

Iron chloride hexahydrate ($FeCl_3\cdot 6H_2O$), zinc chloride hexahydrate ($ZnCl_2\cdot 6H_2O$), ammonium hydroxide (NH_4OH), ethanol (99.5%), and distilled water were used for preparing undoped Fe_2O_3 and zinc-doped Fe_2O_3. Dilute HCl, NaOH, and methanol solutions were used to regenerate the adsorbent for reuse experiments. A standard 2,4-D solution was used to prepare the stock solution of the herbicide, while concentrated sulfuric acid (98%) was utilized for water sample preservation. An electronic balance (ESJ-200-4, Japan), a drying oven (DHG-9070, Japan), and a muffle furnace (Pyrothem Furnace, 6104, Japan) were used for weighing samples, drying, and calcination, respectively. Various volumetric flasks and micropipettes of different capacities were used to measure solutions and reagents. All chemicals were of analytical grade and were utilized without further purification.

2.2. Synthesis of zinc-doped Fe_2O_3 and bare Fe_2O_3

A series of zinc-doped Fe_2O_3 samples (1%, 4%, and 7%) were prepared using a slightly modified co-precipitation method using high-purity chloride precursors of iron and zinc. To prepare the 4% zinc-doped Fe_2O_3, 8.5 g of $FeCl_3\cdot 6H_2O$ and 0.31 g of $ZnCl_2\cdot 6H_2O$ were dissolved in 200 mL of distilled water in a two-necked reaction flask. The mixture was flushed with nitrogen while stirring for 30 minutes on a magnetic stirrer. The products were precipitated at 353 K by adding 30 mL of NH_4OH to maintain a pH of 11, and the mixture was allowed to stand for 3 hours. After centrifugation, the resulting precipitates were washed three times with ethanol and deionized water to remove contaminants. The product was dried at 353 K for 12 hours and then heated at 773 K for 4 hours to obtain pure and Zn-doped α-Fe_2O_3 powders. Undoped α-Fe_2O_3 was synthesized using the same procedure, but without the zinc precursor. The as-prepared samples are designated as UDH, ZDH1, ZDH4, and ZDH7, where UDH refers to undoped hematite, while ZDH1, ZDH4, and ZDH7 denote hematite doped with 1%, 4%, and 7% zinc, respectively.

2.3. Material characterizations

The as-synthesized materials were characterized using various methods, including X-ray diffraction (XRD), scanning electron microscopy (SEM), energy dispersive spectroscopy (EDS), Fourier transform infrared spectroscopy (FTIR), X-ray photoelectron spectroscopy (XPS), and UV-Vis spectrophotometer. The crystallized state of the as-synthesized samples was analyzed using XRD with Cu Kα radiation (λ = 1.5406 Å). To investigate the functional groups present in the samples, a Nicolet NEXUS-670 FT-IR spectrometer was employed. The structural and elemental makeup of the as-prepared samples was analyzed by field emission SEM and XPS, respectively. The amount of 2,4-D during the adsorption process was quantified using a UV-visible spectrophotometer (UV-1800) equipped with 10 mm quartz cells.

2.4. Batch adsorption experiment

Several batch adsorption tests using ZDH4 and UDH as adsorbents were carried out in 100 mL conical flasks. First, the pH of 50 mL of known concentration of 2,4-D solution, which contained 60 mg of adsorbent, was adjusted to 3, 5, 7, 9, and 11 using dilute NaOH and HCl solutions. The resulting mixture was then agitated for 70 minutes at ambient temperature at a speed of 150 rpm. Afterward, a specific volume of the sample was withdrawn, filtered, and the 2,4-D content was measured employing a UV-Vis spectrophotometer at 282 nm. The adsorbent dose, stirring speed, contact time, and initial concentration of 2,4-D were optimized to 15–75 mg, 50–200 rpm, 10–110 min, and 40–200 mg L^{-1} respectively. The effects of coexisting ions were also studied at 298 K. The removal ability of 2,4-D by modified hematite was evaluated using the following formula.

$$\%\text{Removal} = \frac{(C_0 - C_e)}{C_0} \times 100 \tag{1}$$

where C_0 and C_e are the initial and the equilibrium concentration of 2,4-D (mg L^{-1}), respectively. In addition, the adsorption capacity of 2,4-D by modified hematite was obtained employing eqn (2):

$$q_e = \frac{(C_0 - C_e)V}{m} \tag{2}$$

where C_0 (mg L^{-1}) refers to the initial concentration of 2,4-D, C_e (mg L^{-1}) indicates the equilibrium concentration of 2,4-D in the solution, V represents the initial volume of 2,4-D solution employed (in liter), and m denotes the mass of adsorbent (in gram).

2.5. Isotherm, kinetic and thermodynamic studies

Four isotherm models namely Langmuir, Freundlich, Temkin, and Dubinin–Radushkevich were utilized to examine the adsorption process at a temperature of 298 K, with a pH of 3, a contact time of 70 min, an adsorbent dose of 60 mg, and a stirring rate of 150 rpm for different concentrations of 2,4-D (40–200 mg L^{-1}). To determine the rate of adsorption, we employed pseudo-first-order, intra-particle diffusion, pseudo-second-order, and Elovich models at varying contact times. The mathematical expressions for the isotherm, kinetics, and thermodynamic studies are presented in the SI.

2.6. Reusability of Zn–Fe_2O_3 adsorbent

A series of adsorption–desorption trials were performed to examine the retrieval of used ZDH4 and its continued effectiveness in removing 2,4-D. To desorb the spent ZDH4, three solvents were used: 0.1 M HCl, 1 M methanol, and 0.1 M NaOH. Initially, 100 mL of a 120 mg L^{-1} 2,4-D solution was placed in a flask containing 60 mg of ZDH4. The mixture was stirred at 150 rpm and 298 K for 70 minutes. After the adsorption process was complete, the ZDH4/2,4-D solid was recovered by centrifugation, washed with deionized water, and dried in an oven set to 345 K. The dry ZDH4/2,4-D solid was then mixed with 20 mL of solvent and agitated for 70 minutes at 150 rpm. Following agitation, the ZDH4 was filtered and dried for two hours at 333 K before being utilized in the next adsorption cycle to remove 2,4-D. Three replicates of each adsorption and desorption experiment were performed.

2.7. Determining concentration of 2,4-D in real samples

2.7.1. Instrument calibration and method detection limit. To quantify the amount of 2,4-D in real samples, a UV-Vis apparatus was calibrated using five sets of operational standards ranging from 1 to 25 mg L^{-1} under optimal experimental conditions. After successful calibration, we measured the concentration of 2,4-D in real samples, including river water, onions, and potatoes collected from the Akaki River and nearby farming areas, using UV-Vis. The limits of detection (LOD) and quantitation (LOQ) were determined employing the equations provided below:

$$\text{LOD} = \frac{3\delta}{b} \tag{3}$$

$$\text{LOQ} = \frac{10\delta}{b} \tag{4}$$

where, σ is the standard deviation of blank and b is the slope of the linear calibration plot.

2.8. Method validation

The validity of the optimized procedure was verified by spiking a standard concentration of 2,4-D into the samples. The amount of 2,4-D in both spiked and unspiked samples was determined using the calibration obtained from the UV-Vis equipment. The efficiency of the optimized parameters was assessed by adding 0, 15, 60, and 100 mg L^{-1} of 2,4-D standard solutions into 10 mL of pretreated real samples. For instance, adding 1 mL of a 150 mg L^{-1} 2,4-D solution to 10 mL of a real sample resulted in a final concentration of 15 mg L^{-1} of standard 2,4-D.

3. Results and discussion

3.1. Crystallinity and structural studies

The structural and phase studies of the synthesized samples were conducted using an XRD instrument (Fig. 1). Both the doped and undoped samples exhibited four major peaks at 2θ values of 31.7°, 35.3°, 56.4°, and 62.3°, corresponding to the (104), (110), (018), and (214) crystal planes of the rhombohedral hematite structure (JCPDS card no. 84-0311), respectively. Notably, the diffraction peak associated with zinc or zinc oxide was absent in the zinc-doped samples, indicating that zinc atoms were integrated into the α-Fe_2O_3 matrix.[41] A close inspection of the XRD pattern shows no significant changes in peak positions or features when 1% zinc is doped (ZDH1), suggesting that this amount of zinc is insufficient to induce structural

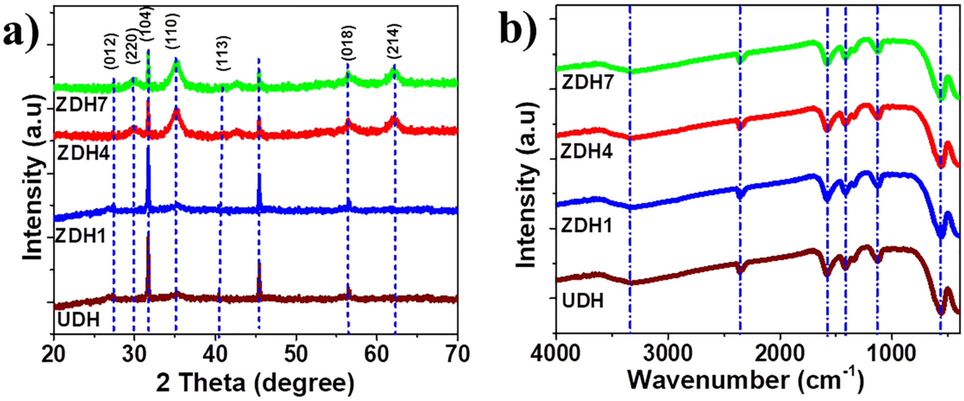

Fig. 1 XRD patterns (a) and FTIR spectra (b) of the UDH, ZDH1, ZDH4, and ZDH7 samples.

changes in hematite. However, when 4% and 7% zinc dopants are incorporated, the XRD pattern shifts slightly to lower angles, and the peaks become broader, particularly at the (110) plane. This further supports the incorporation of Zn^{2+} into the structure of α-Fe_2O_3. To further corroborate these findings, we analyzed the crystallite sizes, lattice parameters, and unit cell volumes of both the bare and zinc-doped samples. The mean crystallite sizes of the synthesized samples were determined using the Scherrer equation, based on the strongest diffraction peak at 31.7° (104). The crystallite sizes of the doped samples decrease up to a 4% Zn concentration, and then slightly increase with further zinc doping (Table S1), indicating that the smaller crystallite sizes result from an improved nucleation in the doped samples.[46] The crystallite sizes slightly increase as the Zn doping increases from 4% to 7%. Additionally, the lattice parameters and unit cell volume, calculated using eqn (2) and (3) in the SI, show a slight increase with increasing Zn-doping (Table S1). This increase is attributed to the replacement of smaller Fe^{3+} ions with larger Zn^{2+} ions, as Zn ions have a slightly higher ionic radius (0.074 nm) compared to Fe^{3+} ions (0.067 nm).

To investigate the frequencies of the functional groups in the synthesized adsorbent, we performed FTIR measurements on the as-prepared materials. Fig. 2(b) displays the FTIR spectra of UDH, ZDH1, ZDH4, and ZDH7, recorded over the range of 4000–400 cm^{-1}. The spectra exhibit several common features, indicating that the fundamental hematite structure is retained across all samples. Characteristic absorption bands around 3415 and 1654 cm^{-1} are ascribed to the stretching of O–H and the bending vibrations of H–O–H, respectively, likely because of adsorbed water or surface hydroxyl groups. The peak at 574 cm^{-1} is attributed to Fe–O lattice vibrations, confirming the presence of the hematite phase. As zinc doping increases, the FTIR spectra of the ZDH samples remain similar to those of UDH; however, a decrease in intensity and a slight shift of peaks to lower frequencies are observed. As depicted in Fig. 2(b), the intensities of the O–H and Fe–O peaks slightly decreased upon doping, suggesting structural modifications within the lattice, likely because of some replacement of Fe^{3+} by Zn^{2+}, which introduces local distortions. A close inspection of Fig. 2(b) reveals a slight shift in the Fe–O and O–H peaks to 568 cm^{-1} and 3411 cm^{-1}, respectively. This slight shift in peak position provides evidence of the incorporation of dopants into the main material, while the reduced peak intensity implies that doping is minimal and only mildly perturbs the Fe–O structural framework.[47]

3.2. Morphological studies

We further examined the microstructure of the as-synthesized materials with varying zinc doping levels using SEM instrument. The SEM images of UDH, ZDH1, ZDH4, and ZDH7 samples are shown in Fig. 2. As shown in Fig. 2(a1)–(a3), the undoped hematite exhibits a heterogeneous morphology, composed of relatively large, well-defined plate-like and spherical particles with smooth surfaces, indicative of good crystallinity. When 1% zinc is doped into the hematite structure, there is no significant change in morphology (Fig. 2(b1)–(b3)). However, a slight reduction in particle size and increased compactness are observed, indicating minor structural modifications without substantial morphological disruption. In contrast, the hematite doped with 4% zinc (ZDH4) exhibits a highly dense, rough surface with relatively smaller particle sizes and increased surface porosity (Fig. 2(c1)–(c3)), which may be favorable for adsorption purposes. Fig. 2(d1)–(d3) presents SEM images of hematite doped with 7% zinc (ZDH7). These images reveal that the particles are highly agglomerated, exhibiting indistinct boundaries and relatively larger sizes with a less porous surface texture. The significant morphological change observed at higher zinc loading maybe attributed to the excessive incorporation of zinc.

3.3. Elemental composition and oxidation state analysis

The elemental makeup and oxidation states of the as-synthesized material were analyzed using XPS. Fig. 3(a) displays the survey spectra of the UDH and ZDH4 samples. The UDH mainly reveals the existence of Fe 2p and O 1s peaks. In contrast, the Zn-doped samples show an additional peak corresponding to Zn 2p, confirming the successful incorporation of zinc into the Fe_2O_3 lattice. The weak carbon and chlorine peaks originate from adventitious hydrocarbons and residual precursors present in the XPS instrument. The core-level spectra of Fe 2p, O 1s, and Zn 2p

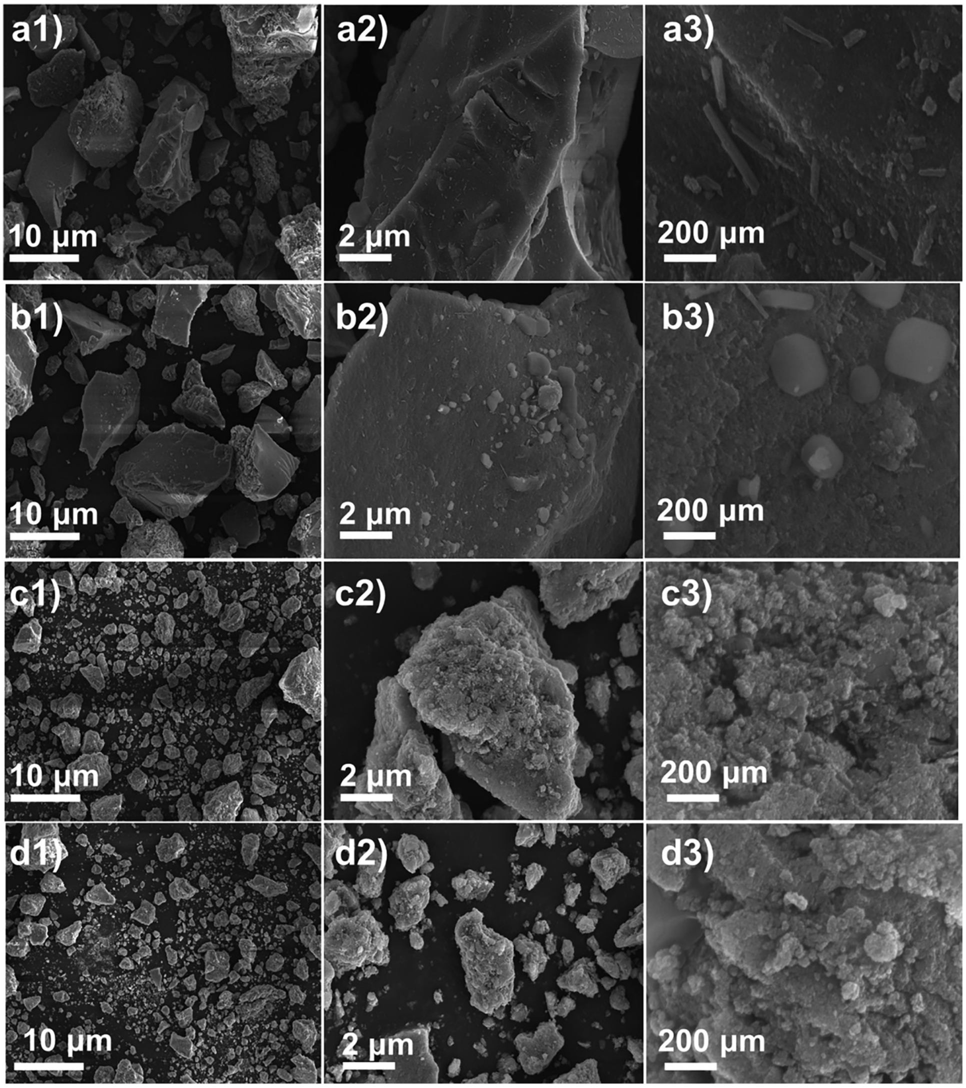

Fig. 2 SEM images of UDH (a1)–(a3), ZDH1 (b1)–(b3), ZDH4 (c1)–(c3), and ZDH7 (d1)–(d3) samples at various magnifications.

for both undoped and zinc-doped samples are indicated in Fig. 3. As displayed in Fig. 3(a), the Fe $2p_{3/2}$ and Fe $2p_{1/2}$ peaks for the undoped sample (UDH) are located at 711.1 eV and 724.8 eV, respectively, suggesting that Fe is in the Fe(III) oxidation state within the hematite structure.[48] Additionally, the observed satellite peak at 719.1 eV, which is about 8 eV higher than the main Fe $2p_{3/2}$ peak, further confirms the presence of trivalent Fe in hematite. The Fe 2p peaks for the zinc-doped hematite samples (ZDH1, ZDH4, and ZDH7) exhibit similar characteristics to those of the undoped hematite; however, the Fe 2p peaks in the zinc-doped samples shift to smaller binding energies, indicating the incorporation of Zn into the hematite structure. This change in binding energy results from electron movement from neighboring Zn atoms to Fe atoms due to the difference in electronegativity between Zn (1.65) and Fe (1.83). We also acquired the XPS spectra for Zn 2p from the ZDH1, ZDH4, and ZDH7 samples (Fig. 3(c)). In these samples, the peaks at 1021.1 eV and 1044.2 eV match-well with divalent Zn $2p_{3/2}$ and Zn $2p_{1/2}$, respectively, suggesting the incorporation of Zn^{2+} into the hematite structure.[49] In contrast to the Fe XPS spectra, the Zn 2p peaks of the ZDH1, ZDH4, and ZDH7 samples are positively shifted compared to the Zn reference. The Zn 2p peaks in the ZDH1, ZDH4, and ZDH7 samples exhibited increased intensity as the Zn loading rose from 1% to 7%, indicating a proportional increase in Zn content. Furthermore, the results from the XPS area ratios show that the Zn and Fe contents in the ZDH1, ZDH4, and ZDH7 samples are in good agreement with the metal precursors' molar proportion employed in synthesis (Table S2). The O 1s XPS spectra for the UDH, ZDH1, ZDH4, and ZDH7 samples are displayed in Fig. 3(d). The main peak, located at 529.7 eV, and a shoulder peak at 531.5 eV are attributed to the hematite lattice and O–H bonds, respectively.[50] The O 1s peaks for the zinc-doped hematite shift to higher binding energies compared to those of the undoped hematite, implying the successful incorporation of Zn into the Fe_2O_3 matrix.

We employed ICP-OES and EDXS to further analyze the elemental composition of the as-prepared materials

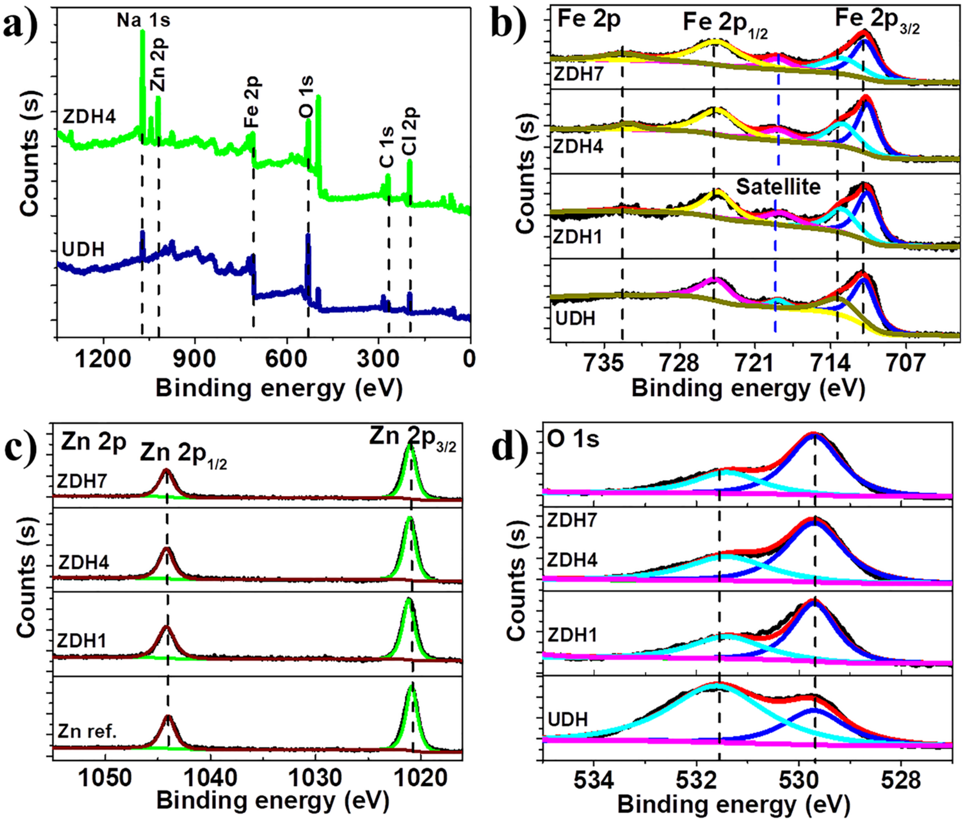

Fig. 3 (a) XPS survey spectra of UDH and ZDH4; high-resolution XPS spectra of Fe 2p (b), Zn 2p (c), and O 1s (d) for UDH, ZDH1, ZDH4, and ZDH7.

(Table S2). The ICP-OES results indicate that the amounts of Fe and Zn in the ZDH samples closely match the molar proportions of the metal sources used during preparation (Table S2). Fig. 4 presents the EDXS elemental mapping from the SEM analysis of the ZDH4 sample. As illustrated in Fig. 4, the elements Fe, Zn, and O are uniformly distributed on the micrometer scale, and their concentrations align with the ICP-OES findings. In contrast, the elemental distribution in undoped hematite was non-uniform (Fig. S1), which may be attributed to the role of zinc in enhancing elemental dispersion during the formation of the hematite phase. To investigate the surface area and pore size distribution of the doped and undoped hematite structures, we conducted N2 physisorption isotherms. As shown in Fig. S2a, the isotherm exhibits type II and type IV behavior, indicating the presence of macro- and mesopores within the adsorbents. The BET surface areas were found to be 28.7 m^2 g^{-1} for the ZDH4 adsorbent and 11.2 m^2 g^{-1} for the UDH adsorbent (Fig. S2a and Table S3). We employed

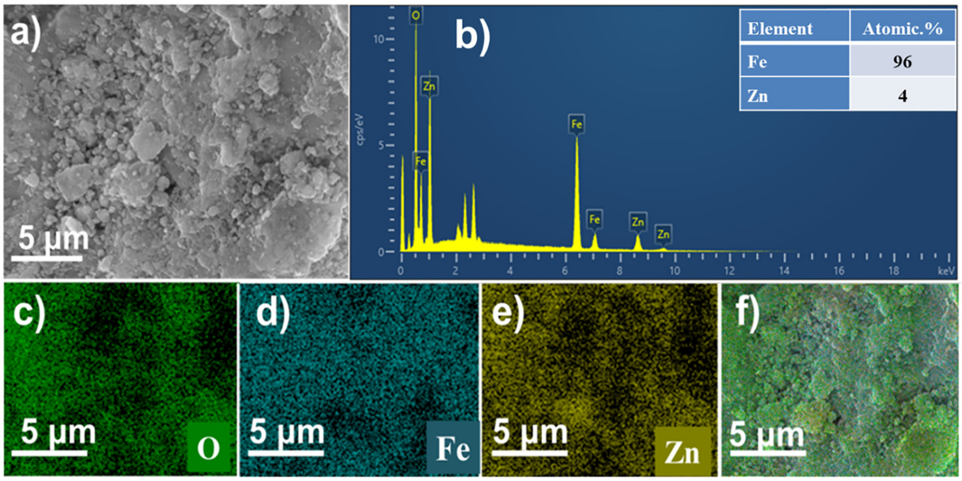

Fig. 4 SEM images (a), EDX spectra (b), corresponding EDX elemental maps (c)–(e), and an overlay of the EDX elemental map for ZDH4 (f).

density functional theory (DFT) to analyze the pore size distributions of the UDH and ZDH4 materials. The UDH sample exhibits only mesopores (2–50 nm). Interestingly, the ZDH4 structure shows a high DFT pore volume for pores ranging from micropores (<2 nm) to mesopores (2–50 nm). Moreover, the disappearance of a plateau at larger P/P_0 values in the sorption isotherm further suggests the presence of macropores (>50 nm) within the samples. The results obtained from the pore size distribution and adsorption isotherms align well with the SEM image analysis.

3.4. Adsorption experiments

3.4.1. Effect of Zn dopant. Bare Fe_2O_3 (UDH) and zinc-doped Fe_2O_3 materials with 1%, 4%, and 7% Zn content (ZDH1, ZDH4, and ZDH7) were synthesized and evaluated for the adsorptive removal of 2,4-D from water and food samples. A calibration curve for 2,4-D concentration was constructed first, demonstrating excellent linearity and a high correlation coefficient, which verifies the accuracy of the analytical method (Fig. S3a). The adsorption efficiency of the four samples was then tested under identical conditions (*i.e.* 120 mg L^{-1} 2,4-D concentration, 60 mg of adsorbent, 70 minutes contact time, 150 rpm shaking speed, and 298 K). The removal efficiencies obtained were 73.6% for UDH, 88.7% for ZDH1, 99.6% for ZDH4, and 89.8% for ZDH7 (Fig. S3b). The highest efficiency observed with 4% Zn-doped Fe_2O_3 is attributed to the optimal level of zinc incorporation, which likely enhances surface characteristics, including porosity, surface area, and the availability of adsorption-active sites. In contrast, the slight decrease in efficiency at 7% doping may result from excessive Zn content, leading to particle agglomeration or pore blockage. These findings suggest that moderate Zn doping significantly improves the efficiency of Fe_2O_3 for the removal of 2,4-D.

3.4.2. Effect of pH and pH_{pzc}. Determining the pH of a solution is fundamental because it affects both the charge distribution of the adsorbent's surface and the ionisation of the adsorbate. To evaluate the surface charge characteristics of the ZDH4 adsorbent, the point of zero charge (pH_{zpc}) was determined. As shown in Fig. 5(a), the pH_{zpc} was found to be 7.3, indicating that the ZDH4 surface is positively charged at pH values below 7.3 and negatively charged above this point. This property directly initiates electrostatic interactions between the ZDH4 and the 2,4-D compounds during the adsorption process. To further support this justification, we calculated the degree of ionization of the 2,4-D molecule. At pH 3, approximately 65.1% of the 2,4-D exists in anionic form, while 34.9% remains in neutral form, based on a pK_a value of 2.73.[51] This suggests that electrostatic interactions are the primary force driving the higher removal efficiency at pH 3. The influence of pH on the elimination 2,4-D was studied by changing the solution pH from 3 to 11 while maintaining other conditions constant: 50 mL of 120 ppm 2,4-D, 60 mg of adsorbent, 70 minutes of contact time, shaking at 150 rpm, and 298 K (Fig. 5(b)). At pH 3, the highest clearance performance of 99.6% was achieved with a notable decline in efficiency at higher pH levels. The superior removal at pH 3 can be attributed to favorable interactions between the partially deprotonated functional groups of 2,4-D and the positively charged surface of ZDH4, as well as the involvement of hydrogen bonding between the surface hydroxyl groups on ZDH4 and the functional groups on 2,4-D. These results are align with previously reported studies.[51,52]

3.4.3. Effect of adsorbent dose. The effect of the adsorbent on the removal of 2,4-D was evaluated by conducting a series of experiments using varying amounts of ZDH4, ranging from 15 to 75 mg (Fig. 5(c)). The adsorption tests were conducted by maintaining the following conditions: a concentration of 120 mg L^{-1}, a contact time of 70 min, a mixing speed of 150 rpm, a temperature of 298 K, a pH of 3, and a batch volume of 50 mL. The results demonstrated a significant increase in

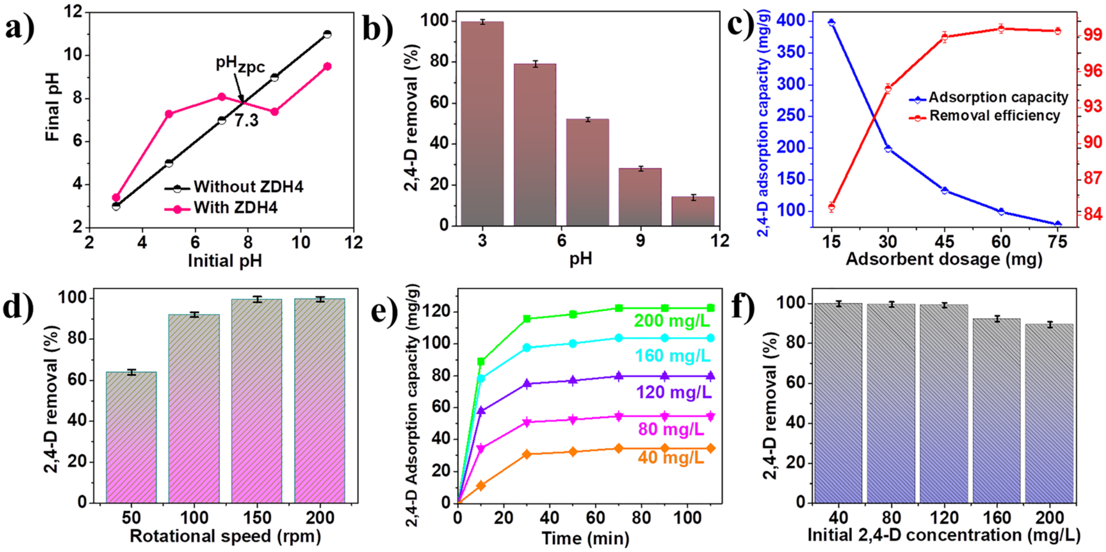

Fig. 5 Zero point of charge profile (a), effects of pH (b), adsorbent dose (c), rotational stirring speed (d), contact time (e), and initial concentration (f) on the adsorption of 2,4-D using ZDH4.

removal efficiency with increasing adsorbent dosage, peaking at 99.6% removal at an optimal dose of 60 mg. The corresponding removal efficiencies at 15, 30, 45, 60, and 75 mg of adsorbent were 84.7%, 94.6%, 98.9%, 99.6%, and 99.4%, respectively (Fig. 5(c)). A slight decrease in removal efficiency was observed beyond the optimal dose, likely due to the aggregation of adsorbent particles at higher dosages, which reduces the effective surface area. The high removal efficiency at the optimal dose can be attributed to the enhanced surface reactivity from zinc doping, which likely introduced additional active sites for the adsorption of 2,4-D. Adsorptive efficiency significantly decreased when the dosage increased from 15 to 75 mg due to the lack of available active sites on ZDH4 for the 2,4-D molecules. These findings align with previous report.[13]

3.4.4. Effect of rotational speed. The performance of ZDH4 in removing 2,4-D was tested at various rotational mixing speeds. Fig. 5(d) illustrates the elimination efficiency of 2,4-D using ZDH4 across mixing speeds ranging from 50 to 200 rpm. The experiments were conducted under optimal conditions. The removal efficiency increased from 64% to 99.5% as the rotational mixing speed was raised from 50 to 150 rpm. This improvement suggests that higher mixing speeds enhance adsorption by facilitating greater interaction between the bulk and solid phases.[53] However, further increases in mixing speed did not significantly impact adsorption efficiency. Therefore, a rotational mixing speed of 150 rpm was selected as optimal for subsequent experiments.

3.4.5. Effect of time and concentration. The impact of time and concentration was conducted by changing the concentrations of 2,4-D (40, 80, 120, 160, and 200 ppm) and contact times (10, 30, 50, 70, 90, and 110 min), while maintaining constant pH, dosage, rotational mixing speed, and temperature at 3, 60 mg, 150 rpm, and 298 K, respectively. As the interaction duration increased from 10 to 70 min, the adsorption capacity rose sharply before leveling off at saturation for all initial concentrations (Fig. 5(e)). The initial increase in adsorption capacity is attributed to the abundance of adsorption sites on the ZDH4 structure available for 2,4-D herbicides. Beyond 70 min, the trend in adsorption capacity stabilized (Fig. 5(e)), indicating that the adsorbent surface had reached saturation, with minimal 2,4-D uptake occurring thereafter. Consequently, 70 min was identified as the optimal contact time for all initial concentrations presented in Fig. 5(e). Furthermore, the performance of ZDH4 in eliminating 2,4-D was assessed by varying the initial concentration of 2,4-D (Fig. 5(f)). The elimination efficiency decreased as the initial 2,4-D concentration increased due to competition among the 2,4-D molecules for the limited active sites on the ZDH4 surface. As a result, as the initial dosage increased, the 2,4-D elimination efficiency steadily decreased.

3.5. Adsorption isotherms

To understand the interaction between adsorbates and adsorbents, we fitted the equilibrium data using four different adsorption isotherm models: Langmuir, Freundlich, Temkin, and Dubinin–Radushkevich (D–R) (Fig. 6). These models explain how 2,4-D molecules distribute between solid and liquid phases at equilibrium. The experimental data were

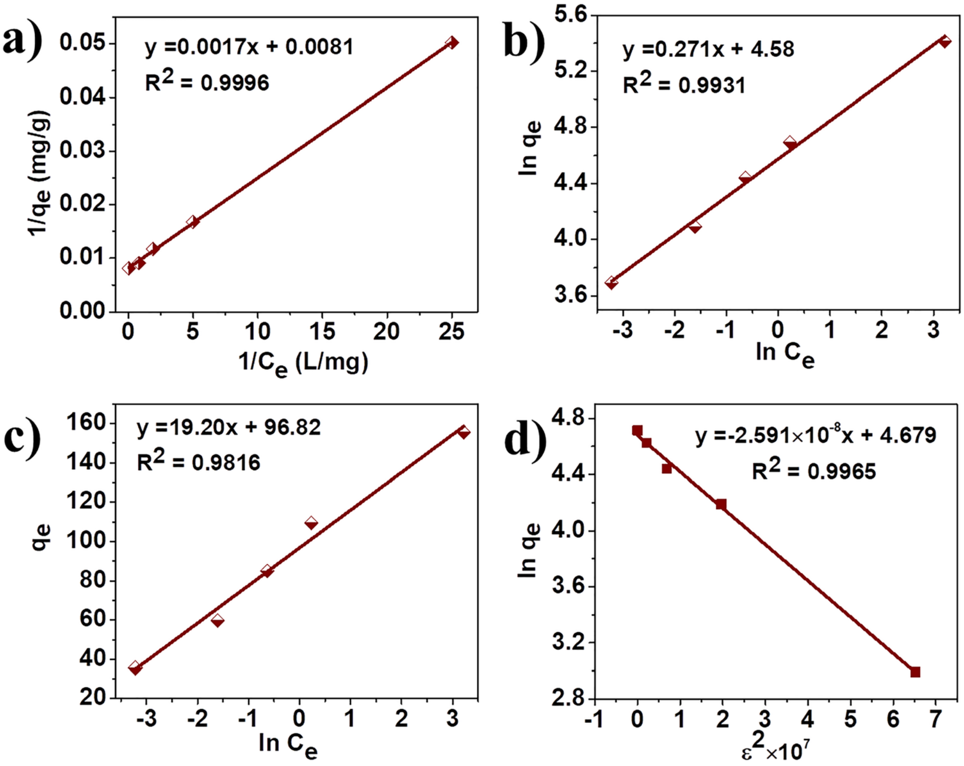

Fig. 6 (a) Langmuir, (b) Freundlich, (c) Temkin, and (d) Dubinin–Radushkevich linearized isotherm models for 2,4-D adsorption onto ZDH4.

collected under optimal conditions: pH 3, a 60 mg adsorbent dosage, an initial 2,4-D concentration of 120 mg L^{-1}, an agitation speed of 150 rpm, a contact time of 70 minutes, and a temperature of 298 K. The equations and parameters for each isotherm model are detailed in Table S4. Each model provides unique insights into the adsorption process: the Langmuir model assumes monolayer adsorption on a homogeneous surface, the Freundlich model accounts for heterogeneous surfaces, the Temkin model considers adsorbate–adsorbent interactions, and the D–R model differentiates between physical and chemical adsorption. The R^2 values were found to be 0.9996, 0.9931, 0.9816, and 0.9965 for Langmuir, Freundlich, Temkin, and D–R models, respectively (Fig. 6). The Langmuir model, which has the highest R^2 value, suggests that the adsorption process predominantly follows monolayer coverage on a uniform surface.[54] The maximum adsorption capacity ($q_{\max}$) and adsorption affinity (b) were determined to be 123.5 mg g^{-1} and 4.76 L mg^{-1}, respectively, indicating high adsorption efficiency and strong interaction between 2,4-D and ZDH4. The order of fit based on R^2 values was: Langmuir > D–R > Freundlich > Temkin, confirming that the Langmuir model best describes the adsorption equilibrium. The high $q_{\max}$ highlights the superior adsorption capacity of ZDH4 compared to many previously reported adsorbents (Table S5). Furthermore, the separation factor (R_L), determined within the concentration range of 40–200 mg L^{-1}, ranged from 0.001 to 0.005, indicating a highly favorable nature of 2,4-D adsorption under the working conditions. According to the D–R model, the mean free energy of adsorption (E) was calculated to be 4392.1 J mol^{-1} (Table S3), suggesting that the adsorption is primarily physical in nature ($E < 8000$ J mol^{-1}). This supports the conclusion that while the adsorption process follows a monolayer mechanism, it is predominantly physisorption.

3.6. Adsorption kinetics and thermodynamics

To analyze the kinetics of 2,4-D on the surface of ZDH4, we conducted kinetic studies under optimal conditions: a concentration of 120 ppm, a temperature of 298 K, a pH of 3, and a stirring speed of 150 rpm. We evaluated the findings using pseudo-first-order (PFO), pseudo-second-order (PSO), intra-particle diffusion (IPD), and Elovich kinetic equations (Fig. 7). Table S6 presents the rate constants, correlation coefficients (R^2), and adsorption capacities for each kinetic model. The R^2 value for the first-order kinetics was 0.9073, demonstrating a relatively poor fit with the pseudo-first-order equation (Fig. 7(a)). In contrast, the data fitted to the PSO kinetic model yielded the highest R^2 value, close to one, signifying that the adsorption of 2,4-D on ZDH4 follows PSO kinetics (Fig. 7(b)). Additionally, the q_e value derived from the PSO model (95.2 mg g^{-1}) closely matched the experimental q_e value (99.5 mg g^{-1}), further confirming the suitability of the PSO model. These results align well with previously published reports. Beyond the PFO and PSO models, we also applied the intra-particle diffusion (Fig. 7(c)) and Elovich (Fig. 7(d)) kinetic models to further explore the rate-limiting steps and the kinetic nature of adsorption on the ZDH4 surface. The corresponding R^2 values from these models were lower than that obtained from the PSO, indicating that the PSO model most accurately describes the adsorption kinetics of 2,4-D on ZDH4.

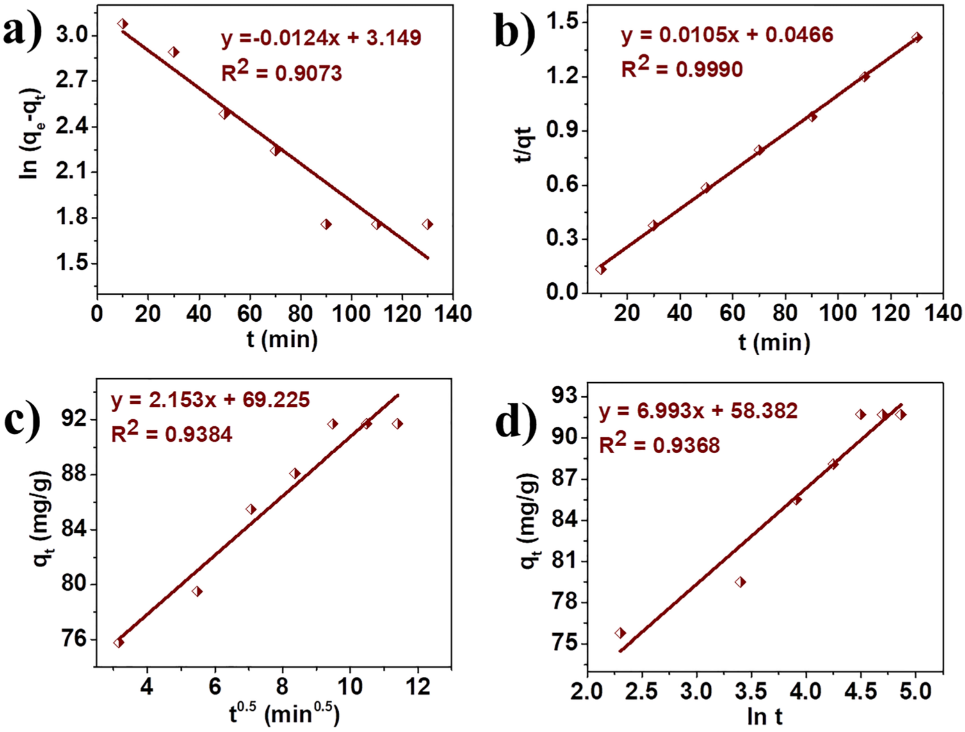

Fig. 7 Kinetic studies for 2,4-D adsorption over the ZDH4 (a) PFO, (b) PSO, (c) IPD and the Elovich model (d).

The influence of temperature was studied by varying it from 298 K to 313 K. The thermodynamic parameters, including the change in standard enthalpy (ΔH°) and standard change in entropy (ΔS°), were obtained from the slope and intercept of the $\ln KT$ *versus* $1/T$ plot (Fig. S4). The negative ΔG° values (Table S7) indicate that the adsorption of 2,4-D onto the ZDH4 adsorbent is spontaneous and feasible, likely due to the high surface area of the synthesized adsorbent.[39] Notably, the ΔG° values decreased with increasing temperature, indicating that adsorption becomes more favorable at higher temperatures. The positive ΔH° (+65.6 kJ mol^{-1}) indicates that the system is endothermic. This value, which falls between 40 and 120 kJ mol^{-1}, suggests that chemisorption occurs during the adsorption process.[55] This conclusion is further supported by the FTIR and XPS findings discussed later. Additionally, the positive ΔS° (+262.7 J mol^{-1} K^{-1}) indicates an increase randomness at the solid–liquid interface, which is favorable for adsorption.

3.7. Effect of coexisting ions

The elimination of 2,4-D, along with coexisting ions that increase ionic strength, is crucial due to the high likelihood of these ions being released into aquatic environments. The selectivity of adsorbents serves as a key performance indicator, and salinity significantly impacts this selectivity. In this study, we examined the effects of varying amounts of common anionic salts (Cl^-, NO^{3-}, SO_4^{2-}, and PO_4^{3-}) and cationic salts (Na^+, Mg^{2+}, and Ca^{2+}) on adsorption under optimal conditions. As illustrated in Fig. S5a, the presence of Ca^{2+} led to slightly higher adsorption efficiency compared to the monovalent Na^+ and divalent Mg^{2+} ions for the same anion (Cl^-), particularly at higher concentrations. This suggests that the greater polarizability of Ca^{2+} enhances the double layer thickness, which is vital for improved adsorption efficiency, unlike Na^+. Conversely, the presence of NO^{3-}, Cl^-, SO_4^{2-}, and PO_4^{3-} ions in water negatively impacted 2,4-D adsorption on 4% Zn-doped Fe_2O_3 compared to conditions without competing anions (Fig. S5b). All tested anions diminished the ability of ZDH4 to remove 2,4-D, with the order of reduction in adsorption capacity being Cl^-, NO^{3-}, SO_4^{2-}, and PO_4^{3-}. Chloride and nitrate ions had minimal effects on the adsorption capacity of 2,4-D, even at higher concentrations. In contrast, SO_4^{2-} and PO_4^{3-} ions significantly hindered adsorption efficiency and capacity at both low and high concentrations. For instance, in the presence of 0.05 M trivalent PO_4^{3-} ions, the 2,4-D adsorption efficiency on ZDH4 decreased to 89%, with adsorption capacity dropping from 123.5 to 116.5 mg g^{-1}. Nevertheless, the adsorption efficiency and capacity of ZDH4 remained approximately 84% and 106.4 mg g^{-1}, respectively, even at higher concentrations of coexisting anions. This indicates that ZDH4 exhibits strong selectivity for 2,4-D.

2.8. Application of the as-synthesized material

To evaluate the applicability of the as-synthesized adsorbent, we determined the concentration of 2,4-D in real samples, including river water, onions, and potatoes, using UV-Vis techniques following the optimized procedure outlined above. The results are presented in Table 1. The concentrations of 2,4-D were found to be 12.4 mg L^{-1} in unspiked river water, 3.2 mg L^{-1} in onion samples, and 1.8 mg L^{-1} in potato samples, indicating that river water exhibited the highest 2,4-D content. The limit of detection (LOD) and limit of quantification (LOQ) were determined to be 1.3 mg L^{-1} and 4.3 mg L^{-1}, respectively. We assessed the efficacy of the as-prepared 4 ZDH4 by examining its ability to remove 2,4-D from the aforementioned real samples. The adsorption efficiency of 2,4-D by ZDH4 was 99.6% for potato samples, 99.2% for onion samples, and 98.9% for river water samples. This demonstrates that the prepared adsorbent effectively removes 2,4-D across a range of concentrations. Additionally, we evaluated the validity of the optimized procedure by spiking a known concentration of 2,4-D into 10 mL of real samples. As shown in Table 1, the recoveries ranged from 98% to 100.2% for river water, 96.7% to 99.8% for onion samples, and 97.7% to 100.1% for potato samples. The average recoveries varied from 97.5% to 100.0%, with an RSD of less than 5%, demonstrating the reliability of the anticipated method for determining 2,4-D in water and food samples. Since the UV-Vis method may be prone to matrix interferences in real samples, future studies should utilize more advanced techniques, such as HPLC-MS or GC–MS, to cross-validate results and improve analytical reliability in practical applications.

Table 1 Recovery value and summary of 2,4-D content in real samples

Samples	Spiked (mg L^{-1})	Actual found (mg L^{-1})	Recovery (%)	RSD (%)
River water	0	12.4	—	0.41
	15	27.1	98.0	3.15
	60	87.2	100.2	2.31
	100	111.9	99.5	4.27
Onion	0	3.2	—	1.32
	15	17.6	96.7	2.73
	60	63.1	99.8	3.54
	100	101.6	98.4	1.77
Potato	0	1.8	—	1.83
	15	14.8	97.7	1.84
	60	59.8	99.4	2.33
	100	100.2	100.1	3.14

3.9. Reusability and adsorption mechanism

We investigated the reusability of ZDH4 to evaluate its stability and economic viability in eliminating 2,4-D from aqueous systems. Various eluent mediums, including 1 M methanol, 0.1 M NaOH, and HCl, were used to regenerate ZDH4 for continuous 2,4-D removal. The adsorption efficacy in the first cycle was highest with the HCl solution (99%), followed by methanol (97%) and NaOH (95%). This suggests that chloride ions in HCl inhibit the interaction between ZDH4 and 2,4-D, leading to the breakdown of the interface and the release of 2,4-D from the adsorbent into the eluent. The adsorption efficacy values for the four cycles using HCl were 99%, 97%, 95%, and 95%, respectively, demonstrating the stability and sustainability of ZDH4 (Fig. S6). The slight decline in efficiency may be attributed to the partial release of adsorbed substances or minor deterioration of the active sites.[52] To confirm the stability of the ZDH4 adsorbent, we conducted ICP-OES tests on aliquots collected from each solution. The results indicated no leaching of zinc or iron from the ZDH4, confirming its high stability.

To examine the adsorption mechanism of 2,4-D on ZDH4, we conducted FTIR, XRD, SEM, and XPS analyses before and after the adsorption test. As shown in Fig. S7a, the O–H peak at 3415 cm^{-1} shifted to 3423 cm^{-1} after adsorption, indicating the formation of hydrogen bonds between 4% Zn-doped Fe_2O_3 and 2,4-D. Additionally, the peaks corresponding to the asymmetric and symmetric stretching of C=O at 1654 and 1485 cm^{-1}, respectively, shifted to 1663 and 1493 cm^{-1} in the ZDH4/2,4-D. These shifts, along with a decrease in peak intensity, suggest that these species play a role in the adsorption process. To further analyze the adsorption mechanism of 2,4-D on ZDH4, XPS measurements were performed before and after adsorption. The atomic composition of Cl 2p increased from 1.63% to 4.32% after adsorption, confirming the adsorption of 2,4-D on ZDH4 (Fig. S7b). The weak C–C signal at 284.57 eV before adsorption, which originates from adventitious hydrocarbons present in the XPS instrument, showed an increase in intensity and shifted to 284.76 eV (Fig. S7c). This change indicates the presence of weak van der Waals forces between ZDH4 and 2,4-D.[9] Additionally, the binding energies for the C–O and O–H peaks, initially at 529.89 eV and 531.90 eV, respectively shifted to 531.01 eV and 532.26 eV, after the adsorption process (Fig. S7d). This shift indicates that charge transfer occurred between 2,4-D and ZDH4.[56] To gain further insight, XRD measurements were conducted on ZDH4 both before and after the adsorption of 2,4-D (Fig. S7d). As shown in Fig. S8a, the XRD patterns exhibit minimal variation between the spectra, with the exception of a slight shift in the peak at $2\theta = 31.7^\circ$ to a lower value. This shift suggests an increase in the *d*-spacing, indicating the adsorption of 2,4-D on ZDH4. The adsorption mechanism is attributed to hydrogen bonding between the carboxyl group in 2,4-D and the oxygen atoms in the adsorbent, along with van der Waals forces and electrostatic interactions (Fig. S9).

4. Conclusion

This study successfully demonstrates the development and application of zinc-doped hematite (ZDH) as a highly efficient adsorbent for removing 2,4-D from aqueous solutions and real-world samples. The optimal dopant level of 4% Zn (ZDH4) significantly enhanced adsorptive performance, achieving a maximum adsorption capacity of 123.5 mg g^{-1}. Detailed characterization confirmed the structural and surface modifications resulting from zinc incorporation, which play a crucial role in improving adsorption efficacy. The Langmuir isotherm best describes the adsorption process, while the kinetics were best analyzed using the pseudo-second-order model. Thermodynamic analyses revealed that the adsorption process is spontaneous, endothermic, and follows a chemisorption-driven mechanism. Additionally, the adsorbent exhibited excellent reusability, maintaining over 95% efficiency after multiple cycles. Remarkably, ZDH4 demonstrated superior performance in real samples, achieving near-complete removal of 2,4-D from river water, onion, and potato matrices. The adsorption mechanism was primarily governed by van der Waals interactions, hydrogen bonding, and electrostatic forces. These findings highlight the potential of ZDH4 as a promising, reusable, and scalable solution for the environmental remediation of herbicide contaminants.

Conflicts of interest

The authors declare that they have no known conflict of interests.

Data availability

The data that support the findings of this study are available from the corresponding author upon reasonable request.

All relevant data used in the analysis have been included in the article and its supplementary information (SI). Supplementary information is available. See DOI: https://doi.org/10.1039/d5ma00985e.

Acknowledgements

Financial support from the Addis Ababa University thematic research project (grant no. TR/525/2023) are gratefully acknowledged.

References

1 M. A. M. Abdelfattah, E. K. Radwan, M. M. Azab, A. A. Aly and W. I. El-Dougdoug, *J. Water Process Eng.*, 2025, **71**, 107304.

2 N. A. Elessawy, A. G. Alhamzani, S. A. J. Almahmoud and B. S. Hsiao, *Ecotoxicol. Environ. Saf.*, 2024, **285**, 117123.

3 D. Sahu, S. Pervez, I. Karbhal, A. Tamrakar, A. Mishra, S. R. Verma, M. K. Deb, K. K. Ghosh, Y. F. Pervez, K. Shrivas and M. L. Satnami, *Desalin. Water Treat.*, 2024, **317**, 100253.

4 I. T. Longchar, S. Kumar, R. S. Umdor, S. Sharma, P. Bora and D. Sinha, *J. Mol. Liq.*, 2024, **415**, 126406.

5 W. M. Moreira, P. V. V. Moreira, T. B. da Costa, M. L. Gimenes and M. G. A. Vieira, *J. Water Process Eng.*, 2023, **54**, 103963.

6 J. Ge, J. Dou, X. Yu, H. Song, Y. Sun and D. Shen, *J. Electroanal. Chem.*, 2024, **970**, 118542.

7 L. Tang, S. Chen, N. Wang and X. Jiang, *Sep. Purif. Technol.*, 2025, **358**, 130470.

8 A. E. Orduz, D. S. do Nascimento, C. Acebal and G. Zanini, *Colloids Surf., A*, 2024, **703**, 135213.

9 H. Wu, L. Gong, X. Zhang, F. He and Z. Li, *Chem. Eng. J.*, 2021, **411**, 128539.

10 S. Li, F. Feng, S. Chen, X. Zhang, Y. Liang and S. Shan, *Ecotoxicol. Environ. Saf.*, 2020, **194**, 110440.

11 D. Franco, L. F. O. Silva, K. de, B. Martinello, J. C. Diel, J. Georgin, M. S. Netto, H. A. Pereira, E. C. Lima and G. L. Dotto, *J. Environ. Chem. Eng.*, 2021, **9**, 106872.

12 M. H. Dehghani, S. Ahmadi, S. Ghosh, M. S. Khan, A. Othmani, W. A. Khanday, Ö. Göokkus, C. Osagie, M. Ahmaruzzaman, S. R. Mishra, E. C. Lima, N. M. Mubarak, R. R. Karri and K. Ansari, *Appl. Surf. Sci. Adv.*, 2024, **19**, 100558.

13 F. M. Mpatani, A. A. Aryee, R. Han, A. N. Kani, Z. Li and L. Qu, *J. Environ. Chem. Eng.*, 2021, **9**, 106714.

14 H. M. Flafel, M. Rafatullah, J. Lalung, R. T. Kapoor, M. R. Siddiqui and M. Qutob, *Chemosphere*, 2024, **367**, 143591.

15 A. Samanth, R. Vinayagam, G. Murugesan, T. Varadavenkatesan, R. Selvaraj and A. Pugazhendhi, *Chemosphere*, 2023, **336**, 139143.

16 A. J. M. Valente, D. Pirozzi, A. Cinquegrana, G. Utzeri, D. Murtinho and F. Sannino, *Environ. Res.*, 2022, **215**, 114214.

17 H. M. Flafel, M. Rafatullah, J. Lalung, R. T. Kapoor, M. R. Siddiqui and M. Qutob, *J. Mol. Liq.*, 2024, **401**, 124754.

18 Q. Li, S. Zhu, R. Yin, X. Ma, G. Li, Y. Yi and F. Dong, *Int. J. Biol. Macromol.*, 2025, **323**, 147040.

19 W. Ma, J. Fan, X. Cui, Y. Wang, Y. Yan, Z. Meng, H. Gao, R. Lu and W. Zhou, *J. Environ. Chem. Eng.*, 2023, **11**, 109165.

20 A. Dargahi, R. Shokoohi, G. Asgari, D. Nematollahic, A. Ansari, D. Nematollahic and M. R. Samarghandi, *RSC Adv.*, 2021, **11**, 9608.

21 B. Liu, N. Guo, Z. Wang, Y. Wang, X. Hao, Z. Yang and Q. Yang, *J. Environ. Chem. Eng.*, 2022, **10**, 107472.

22 S. S. Mohanty, P. Singh, S. Nistala and K. Mohanty, *J. Hazard. Mater. Adv.*, 2024, **16**, 100496.

23 R. Vinayagam, V. Nagendran, L. C. Goveas, M. K. Narasimhan, T. Varadavenkatesan, A. Samanth and R. Selvaraj, *Chemosphere*, 2024, **350**, 141130.

24 C. L. E. Aquino and M. D. L. Balela, *Appl. Sci.*, 2020, **2**, 2099.

25 A. Dargahi, K. Hasani, S. A. Mokhtari, M. Vosoughi, M. Moradi and Y. Vaziri, *J. Environ. Chem. Eng.*, 2021, **9**, 105889.

26 A. Hajighasemkhana, L. Taghavi, E. Moniri, A. H. Hassani and H. A. Panahi, *Int. J. Environ. Anal. Chem.*, 2020, **102**, 1171–1191.

27 X. Dong, J. Deng, M. Ge, S. Lu and Q. Zhu, *Chem. Phys. Lett.*, 2023, **833**, 150950.

28 M. A. Hasan, R. Hossain and V. Sahajwalla, *J. Environ. Manag.*, 2024, **356**, 120461.

29 Y. L. de, O. Salomón, J. Georgin, D. S. P. Franco, M. S. Netto, D. G. A. Piccilli, E. L. Foletto, L. F. S. Oliveira and G. L. Dotto, *J. Environ. Chem. Eng.*, 2021, **9**, 104911.

30 B. A. Oni and S. E. Sanni, *Mater. Today Sustain.*, 2022, **18**, 100134.

31 M. M. Khan, A. Khan, H. N. Bhatti, M. Zahid, S. A. Alissa, Y. A. El-Badry, E. E. Hussein and M. Iqbal, *J. Mater. Res. Technol.*, 2021, **15**, 2016–2025.

32 S. W. Alberti, K. V. Hübner, C. Busso, E. A. da Silva and F. B. Scheufele, *J. Mo. Liq.*, 2023, **382**, 121958.

33 Y. S. Giri, A. Subash and B. Kandasubramanian, *Hybrid Adv.*, 2024, **6**, 100237.

34 T. Gupta, A. Rawat, J. Das, P. K. Sahoo and P. Mohanty, *Sep. Purif. Technol.*, 2025, **360**, 130868.

35 Y. Zhang, Y. Lei, T. Yan, Y. Liao and G. Han, *Sep. Purif. Technol.*, 2024, **334**, 126120.

36 A. A. Alluhaybi, A. Alharbi, K. F. Alshammari and M. G. El-Desouky, *ACS Omega*, 2023, **8**, 40775–40784.

37 T. H. T. Nguyen, K. T. Nguyen, B. H. Le, X. T. Nghiem, D. D. La, D. K. Nguyen and H. P. T. Nguyen, *RSC Adv.*, 2024, **14**, 22304–22311.

38 A. Samanth, R. Selvaraj, G. Murugesan, T. Varadavenkatesan and R. Vinayagam, *Chemosphere*, 2024, **361**, 142513.

39 R. Vinayagam, S. Ganga, G. Murugesan, G. Rangasamy, R. Bhole, L. C. Goveas, T. Varadavenkatesan, N. Dave, A. Samanth, V. R. Devi and R. Selvaraj, *Chemosphere*, 2023, **310**, 136883.

40 N. D. Dien, T. T. H. Pham, X. H. Vu, V. T. Xuan, T. T. T. Nguyen, T. T. Trang, N. V. Hao, P. T. Nga, T. T. K. Chi, T. T. H. Giang and N. D. Toan, *RSC Adv.*, 2024, **14**, 28244–28259.

41 A. Lassoued, *J. Mol. Struct.*, 2021, **1239**, 130489.

42 H. Wang, R. Liu, W. Zhao, J. Zhu, Y. Chen and S. Wang, *Desalin. Water Treat.*, 2023, **298**, 174–183.

43 A. A. khedr, M. E. Fawzy, H. M. Ahmed, S. O. Alshammari and M. A. El-Khateeb, *Desalin. Water Treat.*, 2024, **317**, 100071.

44 X. Wang, J. Gong, W. Tan, T. Hu, R. Rong, Z. Gui, K. Nie and X. Xu, *Nanoscale*, 2020, **12**, 22754–22767.

45 S. Punyasamudram, R. P. Puthalapattu, A. Bathinapatla, S. Kanchi, S. Jyothi and P. V. N. Kumar, *Chem. Phys. Impact*, 2023, **7**, 100282.

46 Z. Dargahi, A. Ahmadi-Arpanah, E. Moradpur-Tari, M. Yarahmadi, M. Kavanlouei, H. Maleki-Ghaleh, D. N. Arator, M. E. Mehr, M. S. Shakeri, J. Paczesny and M. H. Siadati, *Opt. Mater.*, 2024, **157**, 116234.

47 P. Kumar, S. Kumar, A. Tapwal, S. Nimesh and N. Thakur, *Sustain. Chem. Environ.*, 2024, **8**, 100160.

48 P. Guo, S. Li, P. Zhang, S. Luo, Z. Zhao and H. Zhang, *J. Cleaner Prod.*, 2022, **357**, 131991.

49 S. Dong, X. Yan, W. Li, Y. Liu, X. Han, X. Liu, J. Feng, C. Yu, C. Zhang and J. Sun, *J. Ind. Eng. Chem.*, 2022, **108**, 254–262.

50 J. Li, H. Wang, Y. Li, S. Xue and Y. Wang, *Int. J. Electrochem. Sci.*, 2022, **17**, 22106.

51 T. F. Souza, R. L. M. Lobato, J. B. Camargos, G. M. D. Ferreira, J. Ribei-Soares and G. M. D. Ferreira, *J. Environ. Chem. Eng.*, 2024, **12**, 113499.

52 R. Selvaraj, R. V. Iyer, L. C. Goveas, G. Murugesan, T. Varadavenkatesan, A. Samanth and R. Vinayagam, *J. Water Process Eng.*, 2024, **66**, 106027.

53 K. Rambabu, G. Bharath, F. Banat and P. L. Show, *Environ. Res.*, 2020, **187**, 109694.

54 R. Vinayagam, S. Pai, G. Murugesan, T. Varadavenkatesan, S. Narayanasamy and R. Selvaraj, *Chemosphere*, 2022, **286**, 131938.

55 X. Zhang and R. Han, *Environ. Sci. Pollut. Res.*, 2022, **29**, 90738–90751.

56 X. Li, H. Shao, Q. Ma, W. Yu and X. Dong, *Colloids Surf., A*, 2023, **657**, 130519.